Porosity evolution in SnO_2 xerogels during sintering under isothermal conditions

C. V. Santilli and S. H. Pulcinelli
Instituto de Química–UNESP, P.O. Box 355, 14800-900 Araraquara, São Paulo, Brazil

A. F. Craievich
LNLS–Conselho Nacional de Desenvolvimento Científico e Tecnológico, P.O. Box 6192, 13081-970, Campinas, São Paulo, Brazil and Instituto de Física, Universidade de São Paulo, São Paulo, Brazil

(Received 3 October 1994)

The structural evolution during isothermal sintering ($200 \leq T \leq 600$ °C) of SnO_2 xerogels was studied by small-angle x-ray scattering (SAXS) using synchrotron radiation. The SAXS intensity and, consequently, the structure function of the studied samples exhibit, at low q-wave numbers, a sharp decrease for increasing q, and a characteristic peak at larger q values. We associated these two features to the existence of a bimodal size distribution of electronic density heterogeneities related to (i) interaggregate porosity and (ii) internal microporosity, respectively. The maximum of the peak increases with the sintering time in all studied samples. At 300 °C the q value associated with the maximum intensity remains constant. The data analysis of the set of scattering curves for increasing time intervals at 300 °C is in agreement with Cahn's theory for spinodal decomposition. At higher temperatures, 400–600 °C, the maximum of the structure function increases with time, its position shifts continuously to lower q values, and the value of the integrated intensity in reciprocal space remains constant. The structure function of microporous SnO_2 under isothermal treatment in the 400–600 °C range exhibits the dynamical scaling property. The experimental results suggest that the microporosity coarsening is controlled by the coagulation mechanism.

I. INTRODUCTION

The kinetics aspect of phase separation has received considerable attention during recent years[1] due to the relevance of this phenomenon for a wide range of materials including polymers, glasses, metallic alloys, and ceramics. The small-angle x-ray scattering (SAXS) technique is useful for studying this process. It allows, for example, a direct verification of the applicability of Cahn's theory of spinodal decomposition and the statistical dynamical scaling model.[2]

Cahn's theory for phase separation assumes that the boundary between the phases is diffuse, without sharp discontinuities.[3] This theory is based on a Fick diffusion equation with an additional term which accounts for the surface energy associated with the incipient interphases which are formed during the first stages of phase separation. The linear diffusion equation, which is valid for the first stages of the process, was solved for isotropic systems by the Fourier transform method. The result indicates that the structure function $S(q,t)$ and also the SAXS intensity $I(q,t)$ (which is proportional to the structure function) exhibit an exponential growth:

$$S(q,t)=S(q,0)\exp[2Q(q)t]$$

and

$$I(q,t)=I(q,0)\exp[2Q(q)t]\ , \tag{1}$$

where q is the wave number of the scattering vector and "composition wave" and $Q(q)$ is an amplification factor. A qualitative agreement between theory and experiment was observed during the first stages of amorphous phase separation in glasses.[2] To justify some deviations of experiments from the theory, different arguments, such as the influence of nonlinear terms, statistical fluctuations in composition, structural relaxation, and competitive mechanisms, have been suggested.

The classic paper of Lifshitz and Slyozov[4] proposes that the kinetics of growth of domains of the second phase during advanced stages of phase separation is controlled by a coarsening mechanism in which the larger "particles" grow at the expense of the smaller ones. For long periods of time, the asymptotic variation of the average domain size is given by

$$R(t)\propto t^{a}\ , \tag{2}$$

where the exponent a is equal to $\frac{1}{3}$. This type of potential behavior was observed in studies of grain growth in polycrystalline metals and ceramics, a being dependent on the specific model assumptions and on the microscopic mechanisms of the domain, particle, or grain growth.[5]

In analogy with statistical theories for formation of ferromagnetic domains, theoretical studies of phase separation suggest[6–8] that the potential behavior [Eq. (2)] can be explained by a self-similar growth pattern, characterized by a single length scale $R(t)$. After an initial and transient process, $R(t)$ also exhibits a potential behavior and the isotropic structure function $S(q,t)$ satisfies the following scaling property:

$$S(q,t)=R^{d}(t)F(qR(t))$$

and (3)

$$I(q,t)=R^{d}(t)F(qR(t)) ,$$

where d is the dimensionality of the system, q is the modulus of the scattering wave vector, and F is a scaling function. The wide applicability of the dynamical scaling model has been established by computer simulations on two- and three-dimensional models.[7-9] Comparisons with experimental data are limited to studies of phase separation in some binary liquid mixtures,[10] quasibinary glasses,[11] and binary alloys.[12] This fact is partially due to the experimental difficulties of determining the structure function over wide time and length ranges.

Grain and pore growths are verified during the first stages of sintering of porous ceramics such as SiO_2 xerogels,[13] SnO_2 compacted powders,[14] and α-Fe_2O_3 powders.[15] SnO_2 ceramics exhibit large temperature and time ranges in which the volume fraction of pore and solid phase remain constant, which is a necessary condition for the dynamical scaling property of the structure function. A preliminary analysis established the constancy of the volume fraction of the pore growth in SnO_2 porous ceramics[16] in the temperature range 400–1500 °C. This makes SnO_2 ceramics good candidates for testing the applicability of the scaling theory to processes of porosity coarsening also.

This investigation aims at a quantitative verification of the Cahn theory for spinodal decomposition and of the dynamical scaling properties of the structure function associated with porosity evolution in SnO_2 porous ceramics at several temperatures. The porous samples were prepared by a hydrothermal sol-gel route. The parameters associated with the hydrothermal treatment were chosen to obtain amorphous samples with a specially designed texture, i.e., pore and particle size ranges appropriate for the SAXS technique.

II. EXPERIMENTAL PROCEDURES

SnO_2 xerogel samples were prepared by the sol-gel process as described elsewhere.[17] The precipitate was prepared at pH 11 by the addition of NH_4OH to the $SnCl_4$ (0.25 mol dm^{-3}) aqueous solution and submitted to prolonged dialysis to eliminate remnant Cl^- and NH_4^+ ions. After that, peptization of the precipitate occurred, allowing for the formation of a transparent colloidal suspension ([Sn]=0.2 mol dm^{-3}; [Cl^-]$<10^{-5}$ mol dm^{-3}). The sol-gel transition was promoted by partial evaporation of water (60 °C) to reach the critical concentration of sol ([Sn]=0.42 mol dm^{-3}) at which gelation occurs. This process allowed for the formation of a tin oxihydroxide gel, $SnO_{1.2}(OH)_{1.6}$, constituted by primary particles presenting a single-mode size distribution and an initial average size of 3 nm. Aggregation led to 150-nm-length chains.[18] This oxihydroxide was introduced into Pyrex-glass sealed tubes and submitted to hydrothermal treatment in subcritical conditions (250 °C, 52 MPa) for 60 min. This treatment improves the secondary condensation reactions, leading to a decrease in the number of hydroxyl groups, the nominal formula becoming $SnO_{1.8}(OH)_{0.4}$. This strategy was used to improve the chemical and structural homogeneity of the samples. Finally the gel was freeze dried and the powdered xerogel compacted to obtain 0.2-mm-thick slides, by means of a biaxial pressure of 200 MPa.

The SAXS experiments were carried out using the D24 workstation at the synchrotron x-ray source DCI at LURE, Orsay (France). The workstation provided a monochromatic ($\lambda=1.60$ Å) and horizontally focused beam. Two sets of slits were used to define a pinholelike collimated beam. A high-temperature chamber, stable within 1 °C, was used for *in situ* isothermal studies of the xerogel samples during SAXS measurements. The porosity evolution was investigated at 200, 300, 400, 500, and 600 °C. SAXS spectra were recorded a few minutes after placing the sample into the high-temperature cell. A vertical one-dimensional position-sensitive x-ray detector and a standard multichannel analyzer were used to determine the intensity function $I(q)$, in relative units, as a function of the modulus of the scattering vector q. Parasitic air and slit scatterings were subtracted from the total intensity.

An ionization chamber, placed downstream after the sample, was used to monitor the intensity decay of the transmitted beam and to determine the sample attenuation. The natural decay in intensity of the incident beam was monitored by also recording the electronic current in the synchrotron source. Since the electron current intensity as a function of time was proportional to the intensity of the transmitted beam, we concluded that the intensity measured downstream after the sample actually measures the decay of the incident beam without significant interference from scattering effects. This proportionality also indicates that the attenuation of the sample is a constant during the studied process.

Because of the small size of the incident beam cross section at the detection plane, no mathematical desmearing of the experimental data was needed. Each spectrum corresponds to a data collection time interval of 300 s.

III. CRITERIA FOR TESTING THE THEORETICAL MODELS

Equation (1) makes it evident that Cahn's theory for spinodal decomposition can be directly tested with SAXS data. Necessary conditions for the applicability of Cahn's theory are

(i) constant value $q(t)=q_m$ of the position of the maxima in $S(q,t)$ vs q curves;

(ii) exponential variation of $S(q,t)$ as a function of time for every q value; and

(iii) single crossover at $q_c=\sqrt{2}q_m$ of the $S(q,t)$ functions.

In order to verify the dynamical scaling properties of the structure function, we analyzed the time dependence of the unnormalized, $S_n(t)$, and normalized, $q_n(t)$, moments of the structure function, defined as follows:

$$S_n(t)=\int_0^{\infty} S(q,t)q^n dq, \quad n=0,1,2 , \tag{4}$$

and

$$q_n(t)=S_n(t)/S_0(t), \quad n=1,2 . \tag{5}$$

The characteristic size or length $R(t)$ is defined as the inverse of the first normalized moment $1/q_1(t)$. Then Eq. (3) can be written as

$$[q_1(t)]^3 S(q,t) = F(x) \quad \text{where } x = q/q_1 \ . \tag{6}$$

This equation defines the time-independent scaling function $F(x)$.

The unnormalized, $S_n(t)$, and the normalized first moment, $q_1(t)$, of the structure function are related by

$$S_n(t) = K_n [q_1(t)]^{n-2}, \quad n = 0,1,2 \ , \tag{7}$$

where $K_n = \int_0^\infty x^n F(x) dx$. The normalized first moment, $q_1(t)$, and the maximum of the structure function, $S_m = S(q_m,t)$, evolve with time as follows:

$$q_1(t) \propto t^{-a} \tag{8}$$

and

$$S_m \propto t^{a'} \quad \text{where } a' = 3a \ . \tag{9}$$

Because of the invariance of the total volume fraction of phases and dynamical scaling properties, the following quantities remain constant:

$$S_2 = C_1, \quad S_m q_1^3 = C_2, \quad \text{and } q_2/q_1^2 = C_3 \ . \tag{10}$$

For biphasic (two-electronic-density) systems, the time variation of the interface area S_a can be estimated using Porod's law:

$$\lim_{q \to \infty} S(q) \propto (\rho_1 - \rho_2)^2 S_a / q^4 \ , \tag{11}$$

where ρ_1 and ρ_2 are the electronic densities within the phases. When the total volume fractions of the phases are invariant and the difference in electronic density $(\rho_1 - \rho_2)$ remains a constant, the asymptotic value of $S(q)q^4$ $(q \to \infty)$ yields the time variation in relative units of the interface area.

IV. EXPERIMENTAL RESULTS

Time evolutions of the SAXS intensity, measured in relative units during *in situ* isothermal heat treatment at 200, 300, 400, and 600 °C, are shown in Figs. 1(a), 1(b), 1(c), and 1(d), respectively. In a previous study, the SAXS intensity functions corresponding to a sample heat treated at 500 °C were determined.[16] All spectra exhibit

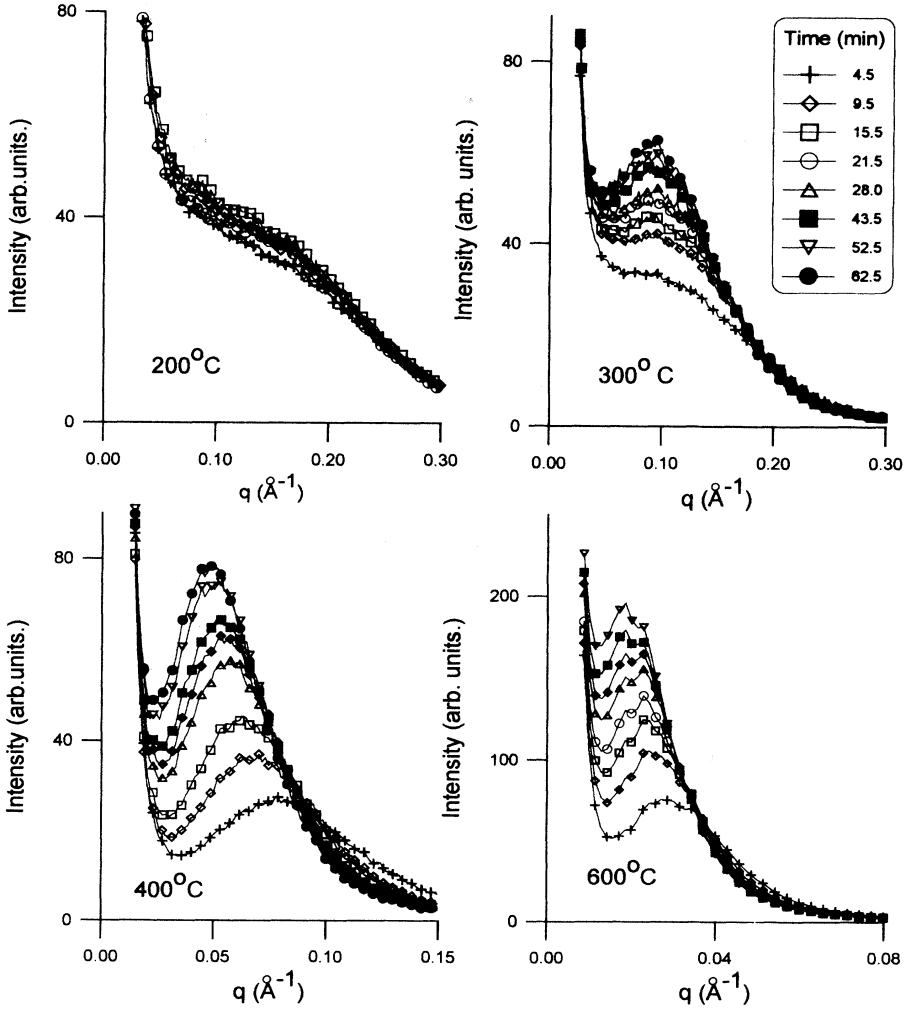

FIG. 1. Time evolution of the SAXS intensity (or structure function) of SnO_2 porous xerogels during *in situ* isothermal sintering at 200, 300, 400, and 600 °C.

two q ranges with clearly different behaviors.

(i) In the low-q range, the SAXS spectra have a sharp decrease for increasing q. This contribution remains essentially invariant with time and temperature of heat treatment. We attributed the origin of this component of the SAXS intensity to the coarse interaggregate porosity.[16]

(ii) In the high-q range, the SAXS spectra have a characteristic peak whose intensity varies with time and is highly dependent on treatment temperature.

At 200 °C, the scattering intensity is almost time invariant [Fig. 1(a)], even after 1 h of isothermal treatment. At 300 °C, the value of the maximum I_m increases with time while the maximum position q_m remains constant [Fig. 1(b)]. Above 300 °C, an increase in I_m and a clear decrease in q_m are observed. The time evolution at 300 °C is qualitatively similar to that predicted for spinodal decomposition associated with phase separation in binary systems. The characteristics of SAXS results for $T > 300$ °C [Figs. 1(c) and 1(d)] are in qualitative agreement with those expected from the theoretical approach for advanced stages of phase separation. In this paper, we focus our attention on the varying part of the scattering functions, which is associated with the structural modifications in the intra-aggregate microporosity of the studied material.

Prior to the calculations of the different moments of the experimental scattering functions, the contribution to SAXS from coarse porosity was subtracted by two different procedures: (i) by extrapolating the low-q range of the total scattering intensity $I_t(q)$ (produced mainly by the coarse porosity), in which the total intensity is described by a power law [$I_p(q) \propto 1/q^4$], and subtracting it from $I_t(q)$ over the whole experimental q range; and (ii) by suppressing the decreasing part of the total scattering function; this part being substituted by a linear extrapolation between a minimum value of $q = q_{\min}$, selected for each curve, and $q = 0$ assuming $I(0) = 0$. $I(q)$, $I(q)q$, and $I(q)q^2$ were integrated numerically between $q_{\min}$ and the maximum experimental value of q, $q_{\max} = 0.18$ Å, for which the intensity function obeys Porod's law. For $q > q_{\max}$, the integrations were carried out analytically after extrapolations of the q^{-4} dependence. The total integrals yielded S_0, S_1, and S_2. The two procedures for the subtraction of $I_p(q)$ led to slightly different numerical values but both exhibited essentially the same variation with time.

Figure 2 shows the log-log plots of the normalized first moment $q_1(t)$ as a function of time for samples treated isothermally at 200, 300, 400, 500, and 600 °C. We note a linear behavior for all temperatures. At $T = 200$ °C q_1 is time independent. For $T = 300$ °C, a weak decrease in q_1 is observed.

The experimental results of Fig. 2 concerning the samples heat treated about 300 °C indicate that the theoretical prediction specified by Eq. (8) is obeyed. The values of the exponents a are about the same for samples treated at 400 °C and 500 °C ($a = 0.15$ and 0.16, respectively) and slightly lower for those treated at 600 °C ($a = 0.13$).

The approximate invariance of the exponent observed

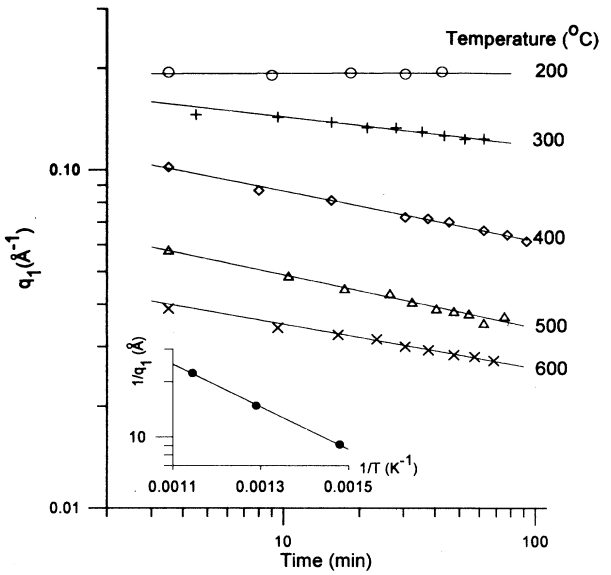

FIG. 2. Log-log plots of the normalized first moment $q_1(t)$ as a function of time of sintering. The insertion shows the values of $1/q_1(t)$ extrapolated to the origin as a function of the reciprocal temperature.

for $T \geq 400$ °C allowed us to determine the activation energy of the growth process characterized by the length $R(t) = 1/q_1(t)$. The values of $1/q_1$ extrapolated to $t = 0$, for the different temperatures, are presented in an Arrhenius plot in the inset of Fig. 2. A least-squares fitting of a straight line yields a value of 22 kJ mol^{-1} for the activation energy of $R(t)$ growth.

The time variations of the maximum of the scattered intensity S_m for samples treated at 300, 400, 500, and 600 °C are presented in Fig. 3 on logarithmic scales. The linear behavior observed is in agreement with Eq. (9). For samples treated at 400, 500, and 600 °C, the slope a' is approximately equal to $3a$ as predicted by Eq. (9) (the exponents a' are equal to 0.34, 0.46, and 0.35 for temperatures of 400, 500, and 600 °C, respectively). The equation $a' = 3a$ is approximately obeyed for samples heat treated at 500 °C. The exponent a' is somewhat lower than $3a$ for $T = 400$ and 600 °C.

Figure 4 shows the log-log plots of the moments $S_0(t)/S_0(t_f)$, $S_1(t)/S_1(t_f)$, $S_2(t)/S_2(t_f)$, and $q_2(t)/q_2(t_f)$ as functions of $q_1(t)/q_1(t_f)$, where t_f corresponds to the longest time at each temperature. The linear theoretical behavior predicted by Eq. (5) is apparent for all moments corresponding to temperatures of 400, 500, and 600 °C. Data concerning samples treated at 200 and 300 °C present a considerable deviation from the theoretical behavior and are not shown in the figure. The invariance of S_2, observed in Fig. 4, indicates that the volume fraction and electronic density of both phases remain constant during heat treatment. Under these conditions, the time variation of the interface area S_a is proportional to the asymptotic value of $S(q)q^4$ of the corresponding SAXS curves [Eq. (11)]. In Fig. 5, the time evo-

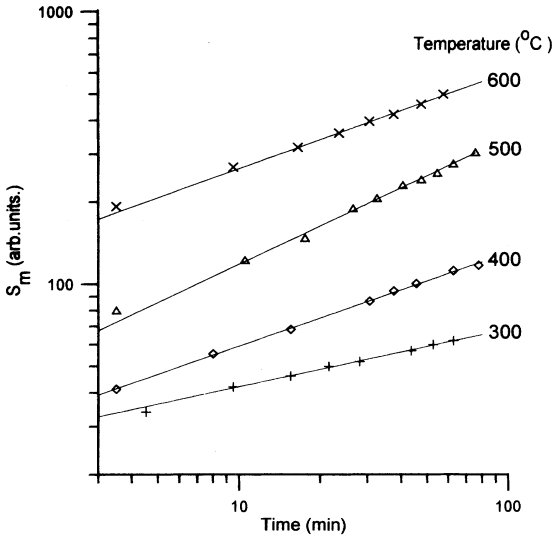

FIG. 3. Time dependence of the maximum of the structure function, S_m, on a double logarithmic scale.

lution of the ratio $S_a(t)/S_a(0)$ is plotted, where $S_a(0)$ is the asymptotic value of $S(q)q^4$ of the sample without thermal treatment. For all temperatures, a monotonic decrease of interface area is apparent, as expected for a coarsening mechanism of porosity evolution.

The plots of q_2/q_1^2 and $S_m q_1^3$ as functions of time of

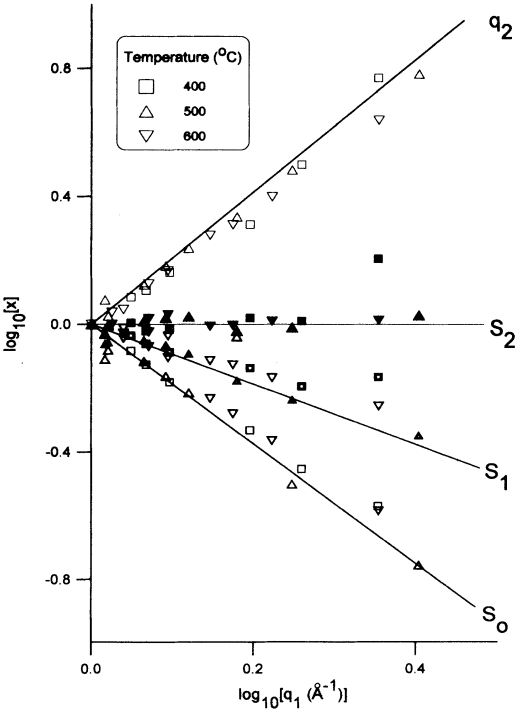

FIG. 4. Log-log plots of the moments $S_0(t)/S_0(t_f)$, $S_1(t)/S_1(t_f)$, $S_2(t)/S_2(t_f)$, and $q_2(t)/q_2(t_f)$ as functions of $q_1(t)/q_1(t_f)$, where t_f is the longest time of sintering. The straight lines have the slopes predicted by the theory (-2, -1, 0, and 2, respectively).

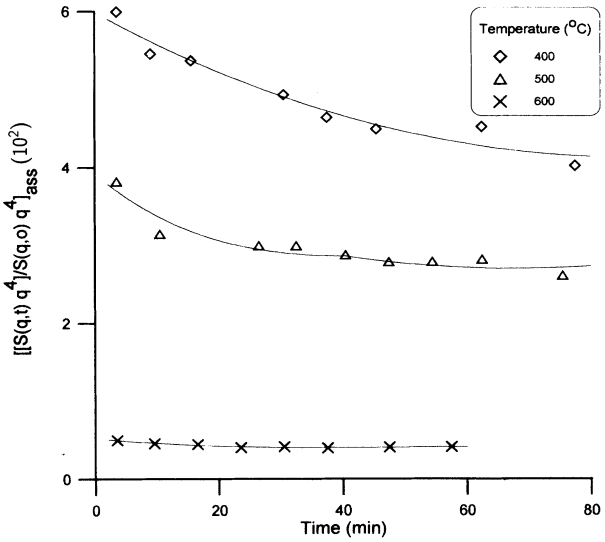

FIG. 5. Time evolution of $S_a(t)/S_a(0)$, where $S_a(0)$ is associated with the asymptotic value of $S(q)q^4$ [Eq. (11)] for the sample without heat treatment.

isothermal treatment at 300, 400, 500, and 600 °C are shown in Figs. 6(a) and 6(b), respectively. As the intensity measurements were carried out in relative units, their values were normalized, dividing by the time-independent moment S_2, in the whole q range. The time invariances of q_2/q_1^2 and $S_m q_1^3/S_2$ are other experimental evidences

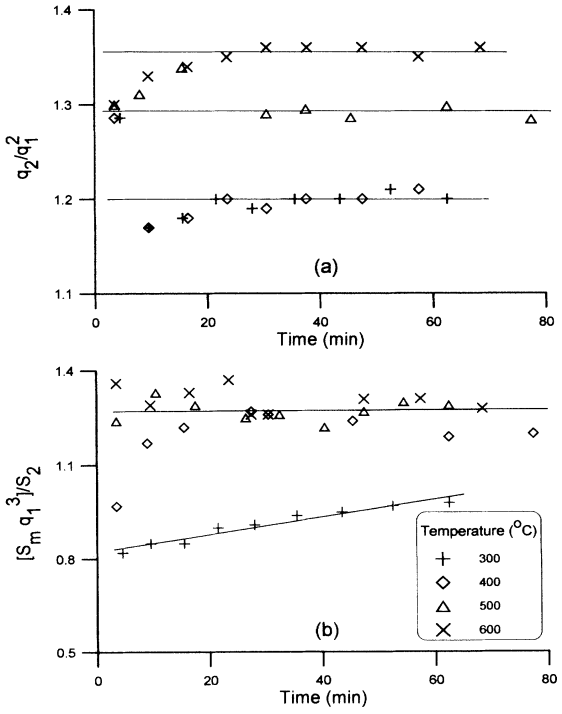

FIG. 6. Time dependences of q_2/q_1^2 and $S_m q_1^3$ for samples sintered at 300, 400, 500, and 600 °C.

for the applicability of the dynamical scaling theory [Eqs. (10)] to the studied porous system heat treated above 300 °C. These conditions are not fulfilled by the sample treated at 300 °C, for which a clear continuous increase of $S_m q_1^3$ occurs.

The normalized experimental structure functions at 400 and 600 °C are plotted in Fig. 7 as $S(q,t)q_1^3(t)/S_2$ versus q/q_1. With the exception of the first $F(x)$ function, corresponding to the initial states of the evolution, all others are actually time independent. This implies that, except during the very early stages of the process, the dynamical scaling model applies to the studied system.

Taking into account all the above-mentioned experimental results, it is apparent that the dynamical scaling model does not hold for the porous samples treated at 200 and 300 °C. Since, for these temperatures, the studied system is in its initial stage of porosity evolution, we tried to verify the applicability of Cahn's theory for spinodal decomposition. The SAXS intensities associated with microporosity in the sample treated at 300 °C are shown in Fig. 8. Due to the relatively strong contribution of coarse porosity to the total scattered intensity, it was not possible to accurately determine the q_m and q_c values for samples treated at 200 °C. One of the vertical dashed lines in Fig. 8 clearly shows that q_m (position of the maxima) is time invariant. A crossover of experimental SAXS functions, q_c, is observed for $t > 9.5$ min. The experimental intensities for $t < 9.5$ min do not have a defined crossover. Moreover, for long treatment time the ratio q_c/q_m is equal to 1.76 instead of 1.41 as predicted by Cahn's theory.

The time evolution of the structure function at several values of the composition wave number q is shown in Fig. 9, for the sample treated at 300 °C. The linear time dependence of $\log S(q)$, which is apparent for $t > 10$ min, agrees with Cahn's theory for spinodal decomposition [Eq. (1)]. For $q < q_c$, the amplitude of the composition wave increases and for $q > q_c$ it decreases, in agreement with Cahn's theory. However, the experimental results for very short times deviate from linear behavior.

Table I groups some structural parameters, determined by means of experimental techniques other than SAXS, for samples treated at several temperatures. These parameters are the real and bulk density (determined by He and Hg pycnometry, respectively), total pore volume, average pore size, and specific surface area, determined by N_2 isothermal adsorption, and average crystallite size (obtained from x-ray-diffraction peak width). It is interesting to note the increase in crystallite and pore sizes, and the large decrease in the surface area, for increasing sintering temperature.

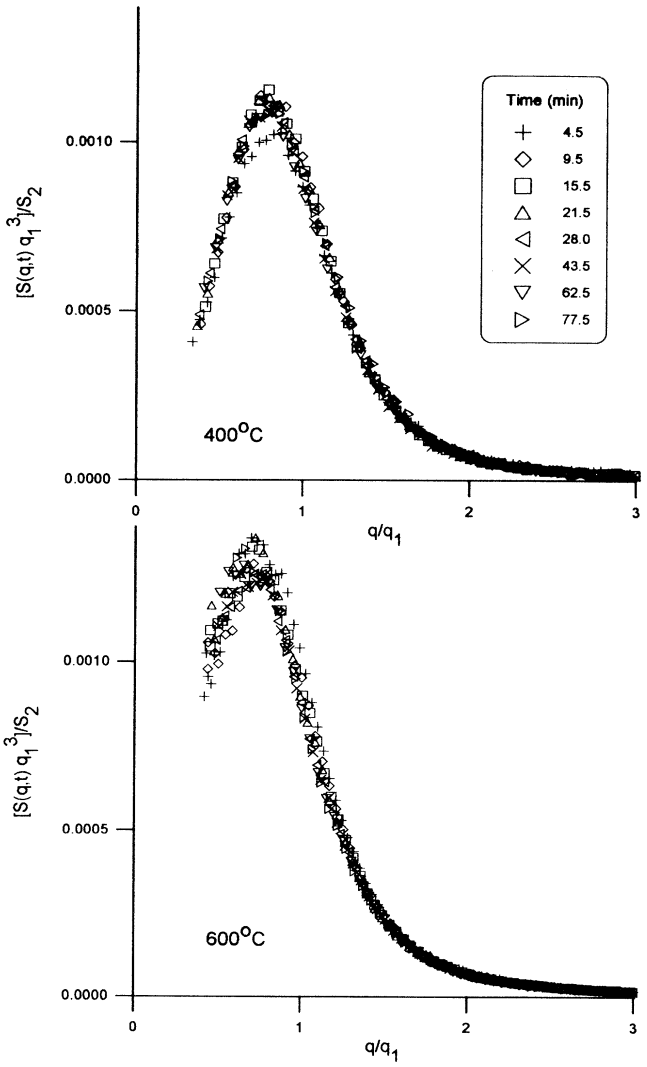

FIG. 7. Dynamical scaling behavior of the experimental structure function of the samples sintered at 400 and 600 °C.

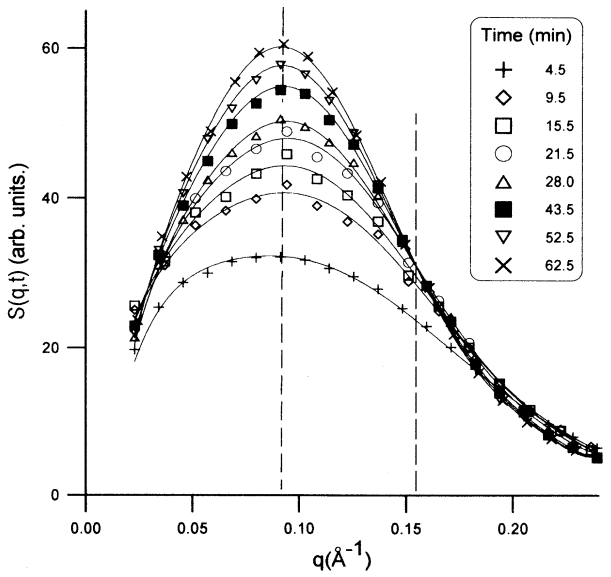

FIG. 8. Structure function corresponding to the micropores as a function of q for the sample treated at 300 °C. Vertical dashed lines indicate q_m and q_c values.

TABLE I. Time evolution of the structural characteristics of xerogels sintered for 10 and 30 min. (*) Bragg peaks are not well defined.

T (°C)	Time (min)	Density (g cm^{-3}) Real	Bulk	Pore volume (cm^2 g^{-1})	Surface area (m^2 g^{-1})	Average size (nm) Pore	Crystallites
110	1080	5.07	4.11	8.6	184	1.7	*
400	10	6.27	4.01	9.0	125	2.9	13
400	30	6.29	4.04	9.1	104	3.5	14
600	10	6.45	4.10	8.8	36	9.6	30
600	30	6.48	4.12	9.0	36	10.6	33

V. DISCUSSION

Basically, SAXS experimental results show two different behaviors: (i) at $T=300$ °C, a good agreement between the experimental results and Cahn's theory for spinodal decomposition was observed for time of heating higher than 15 min, the behavior observed in the early times being due to a transient structural effect, which will be discussed in the next section, and (ii) for the temperature range of $400 \leq T \leq 600$ °C, a general agreement with the statistical theory which predicts the dynamical scaling property of the structure function was observed. We should recall that both theories were established for phase-separation phenomena but they apply to different stages of the process: Cahn's theory is an approximation for early stages and the dynamical scaling model holds for advanced ones. We will discuss both sets of results (at 300 °C and in the range 400–600 °C) separately.

Low-temperature process (300 °C)

From the analysis of the experimental data corresponding to 300 °C, and their comparison with Cahn's theory, two regimes for the time evolution of the structure function are apparent. The first one (short-time regime) is characterized by a varying slope in $\log S(q,t)$ versus t plots for small q (Fig. 9). The q_m values are constant while q_c decreases. For longer times a crossover of the $S(q)$ functions and a linear dependence of $S(q)$ on t are observed, as can be seen in Figs. 8 and 9, respectively, in agreement with Cahn's model. The only deviation from the basic theoretical predictions is the value of the ratio $q_c/q_m=1.76$ which is higher than expected $(q_c/q_m=1.41)$.

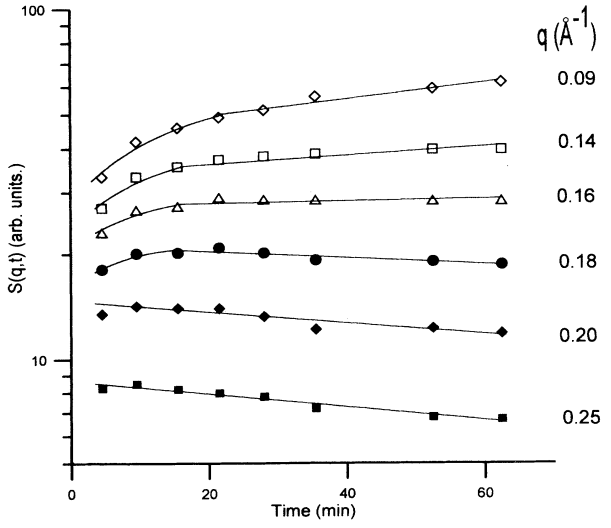

FIG. 9. Time evolution of the structure function at several indicated q values for the sample heat treated at 300 °C, in a double logarithmic scale.

Most of the previous experimental investigations revealed that the basic Cahn equation for spinodal decomposition does not accurately describe the first stages of phase separation. In order to explain the deviation, Cook[19] introduced a modification in Cahn's equation[3] associated with statistical composition fluctuations within the phases. The solution to the modified equation leads to a value of the quotient q_c/q_m higher than 1.41. Therefore statistical fluctuations may explain the experimental value of $q_c/q_m=1.76$ which is higher than that expected from the original Cahn theory. A more quantitative analysis of the effect of statistical fluctuations requires the measurement of SAXS intensity in absolute units.

Deviations from linearity of $\log S(q)$ versus t plots during the first stages of separation in borate glasses were attributed to the existence of transient elastic strains associated with the quenching of the samples.[20] In the disordered matrix of SnO_2 xerogels at temperatures close to 300 °C, the nucleation of an ordered (crystalline) phase occurs. This is followed by a change in the sample composition, due to the loss of remnant OH groups, and by a consequent increase in real density (Table I). Doherty[1] suggests that this transformation produces elastic strains hindering crystallization. These strains are probably responsible for the increase, at short times, of the amplification factor Q and, consequently, of the slopes of $\log S(q,t)$ versus t plots. Due to a progressive stress relaxation, the amplification factor would decrease and eventually become a constant for advanced stages at 300 °C as shown in Fig. 9.

High-temperature process

The analysis of the experimental results associated with heat treatments at 400 °C and above makes apparent the validity of the dynamical scaling model for the structure function of SnO_2 porous xerogels. As expected, deviations from the scaling behavior [Eq. (9)] have been ob-

served at low temperatures ($T \leq 300\,^{\circ}C$) and during the first minutes of heat treatments at 400, 500, and 600 °C. That means that (i) at 300 °C, the porosity evolution corresponds to initial stages, even for the highest time, and (ii) during the early stages at 400, 500, and 600 °C, the matrices still have varying composition and/or volume fractions. A transient short-time effect is observed for the values of pore volumes and real densities (see Table I). The increase in real densities with time would indicate that nucleation of an ordered phase (crystallization) occurs during the first stages, leading to the transient increase in the pore volume fraction. We should recall that the dynamical scaling model applies to two-density systems with constant composition and volume fractions.

Additional evidence of the validity of the scaling hypothesis is given by the values of a and a', the time exponents defined by Eqs. (8) and (9). The expected relation $a'=3a$ is obeyed for $T=500\,^{\circ}C$ and approximately verified for $T=400$ and 600 °C. Differences between a' and $3a$ observed for some metallic systems were attributed to crystal anisotropy.[1]

The time exponent of the characteristic length $R(t)$ is an approximately constant value close to 0.16 at 500 °C and slightly lower at 400 and 600 °C. This value is expected for a mechanism of phase growth controlled by cluster coagulation. Computer simulations[9] demonstrated that this mechanism occurs predominantly during the last stages of phase separation in binary systems with composition near the center of the miscibility gap in which the volume fraction of phases is close to 0.50. In the studied SnO_2 xerogel, we have approximately 45% of porous phase and 55% of solid phase. These values are similar to those expected for the part of the miscibility gap associated with two-phase separation. Moreover, the time evolution of the shape of the structure function (Fig. 1) and the considerable broadening of the scaled structure function (Fig. 7) are analogous to those observed for glass samples close to the center of the miscibility gap. Thus the results obtained for SnO_2 porous xerogels seem to indicate that the validity of the dynamical scaling model is not restricted to phase separation in crystalline or amorphous binary or quasibinary mixtures, but has a more universal character, also including structural evolutions in porous systems.

Specifically concerning the microstructure evolution of the studied SnO_2 ceramics during the sintering process, several mechanisms have been proposed in the past to explain the observed pore and grain growth. Some authors have attributed this phenomenon to a process controlled by diffusion,[21–23] whereas others to a nondiffusional process, like evaporation-condensation.[24,25] The good agreement between experimental SAXS data and phase-separation theories allows us to conclude that the basic process for structure evolution in porous SnO_2 xerogels is vacancy diffusion associated with the coagulation mechanism. However, the value of 22 kJ mol^{-1} for the activation energy for the growth of the characteristic length, $R(t)$ is smaller than that observed for diffusion in crystalline oxides. This low value may be due to the high concentration of vacant sites resulting from the evaporation of volatiles during drying and to the poor crystallinity of the samples. For TiO_{2-x} (isomorphic to SnO_2), for example, the activation energy of a diffusion-controlled process changes continuously from 280 kJ mol^{-1} for $x=0$ to 137 kJ mol^{-1} for reduced rutile with composition corresponding to $x=0.01$. Moreover, dissolved hydrogen may greatly affect the properties of rutile-type compounds; when hydrogen-doped rutile is heated, the loss of water molecules leads to the formation of oxygen vacancies.[26] For SnO_2 xerogels, thermogravimetric analysis shows a small and continuous loss of water; this may contribute to a high vacancy concentration and explain the decrease in the activation energy of the diffusional process.

VI. CONCLUSION

The presented SAXS results indicate that the structural modifications in the microporosity of SnO_2 xerogels can be described by classical models which are currently applied to phase separation in alloys, glasses, and polymers. After a transient behavior, the structural modifications in SnO_2 xerogels, under isothermal conditions at different temperatures, follow two different kinetic models.

(i) At low temperatures ($T=300\,^{\circ}C$) SAXS results are in good agreement with the predictions of Cahn's theory for spinodal decomposition.

(ii) At high temperatures ($400 \leq T \leq 600\,^{\circ}C$) the experimental SAXS results are in accordance with the model of dynamical scaling.

These results suggest that a SnO_2 xerogel, heat treated in the temperature range 400–600 °C, may be seen as a two-phase system composed of (i) a nearly homogeneous SnO_2 matrix containing a high vacancy concentration, and (ii) empty microvoids, the total volume fraction being time constant and the structural variation governed by vacancy diffusion.

Under these conditions of structural transformation, no significant densification occurs. Efficient sintering leading to the effective reduction or elimination of voids requires other mechanisms which are active at much higher temperatures (above 1500 °C for SnO_2). For this type of densification process, the models proposed for low temperatures ($200 \leq T \leq 600\,^{\circ}C$), obviously, do not apply.

These SAXS results strongly suggest that Cahn's model for spinodal decomposition and the model which predicts the dynamical scaling property of the structure function, derived from basic thermodynamic and statistical considerations for simple binary solid solutions, have a more universal domain of applicability. They are also useful for understanding the processes involved in structural transformations in microporous materials.

ACKNOWLEDGMENTS

The authors thank L. R. B. Santos and G. E. S. Brito for the sample preparation and FAPESP (Fundação de Amparo à Pesquisa do Estado de São Paulo, Brazil) and CNPq (Brazilian National Science Council) for financial support. One of the authors (A.F.C.) thanks J. M. Sanchez for useful comments.

[1]R. D. Doherty, in *Physical Metallurgy,* edited by R. W. Cahn and P. Haasen (North-Holland, Amsterdam, 1983), pp. 933–1030.
[2]A. F. Craievich, E. D. Zanotto, and P. F. James, Bull. Mineral. **106**, 169 (1983).
[3]J. W. Cahn, Acta Metall. **9**, 795 (1961).
[4]I. M. Lifshitz and V. V. Slyozov, J. Phys. Chem. Solids **19**, 35 (1961).
[5]D. B. Assolant, *Chimie-Physique du Frittage* (Editions Hèrmes, Paris, 1993).
[6]J. S. Langer, Ann. Phys. (N.Y.) **65**, 53 (1971).
[7]J. Marro, J. L. Lebowitz, and M. H. Kalos, Phys. Rev. Lett. **43**, 282 (1979).
[8]A. Sadiq and J. Binde, Stat. Phys. **35**, 517 (1984); Phys. Rev. Lett. **51**, 674 (1983).
[9]J. M. Houlrik and S. J. K. Jensen, Phys. Rev. B **34**, 7828 (1986).
[10]Y. C. Chou and W. I. Goldburg, Phys. Rev. A **23**, 858 (1981).
[11]A. F. Craievich, J. M. Sanchez, and C. E. Williams, Phys. Rev. B **34**, 2762 (1986).
[12]S. Katano and M. Iizumi, Phys. Rev. Lett. **52**, 835 (1984).
[13]A. Craievich, T. Lours, and J. Zarzycki, in *Anais do VIII CBECIMAT,* edited by C. Zavaglia, I. Torriani, and E. Bresciani (Unicamp, Campinas, 1988), pp. 504–507; T. Lours, Ph.D. thesis, Université de Montepellier, 1988.
[14]G. E. S. Brito, S. H. Pulcinelli, C. V. Santilli, and N. Barelli, J. Mater. Sci. Lett. **12**, 992 (1993).
[15]C. V. Santilli, M. Onillon, and J. P. Bonnet, Ceram. Int. **16**, 89 (1990).
[16]A. F. Craievich, C. V. Santilli, and S. H. Pulcinelli, Nucl. Instrum. Methods Phys. Res. Sect. B (to be published).
[17]R. S. Hiratsuka, S. H. Pulcinelli, and C. V. Santilli, J. Non-Cryst. Solids **121**, 76 (1990).
[18]S. H. Pulcinelli, C. V. Santilli, J. P. Jolivet, and E. Tronc, J. Non-Cryst. Solids **170**, 21 (1994).
[19]H. E. Cook, Acta Metall. **18**, 297 (1970).
[20]A. F. Craievich, Phys. Status Solidi A **28**, 609 (1975).
[21]F. Quadir and D. W. Ready, in *Sintering and Heterogeneous Catalysis,* edited by G. C. Kuczynsk (Plenum, New York, 1984), p. 159.
[22]G. E. S. Brito, C. V. Santilli, and S. H. Pulcinelli (unpublished).
[23]J. F. Goodman and S. J. Greeg, J. Chem. Soc. **82**, 1162 (1960).
[24]J. A. Varela, O. J. Whittemore, and E. Longo, Ceram. Int. **16**, 177 (1990).
[25]H. O. Joss, MS thesis, University of Washington, 1975.
[26]P. Kofstad, *Nonstoichiometry, Diffusion and Electrical Conductivity in Binary Metal Oxides* (Krieger, Malabar, 1983), pp. 139–152.